IJMTARC – VOLUME – IX – ISSUE – 36, OCT - DEC, 2021

ISSN: 2320-1363

DC FAULT PROTECTION AND POWER OSCILLATION DAMPING USING NON LINEAR ALGORITHMS UNDER WAMS

[1]A. UDAYAKUMAR, [2]M. PRADEEP

[1] PG SCHOLAR, POWER SYSTEMS ENGINEERING, DEPT OF EEE, PRIYADARSHINI ENGINEERING COLLEGE, CHETTIYAPPANUR VILLAGE, VANIYAMBADI.

[2] ASSISTANT PROFESSOR, DEPT OF EEE, PRIYADARSHINI ENGINEERING COLLEGE, CHETTIYAPPANUR VILLAGE, VANIYAMBADI.

ABSTRACT

This project is applicable to multi-agent system (MAS)-based distributed control model, which contains a top layer communication network and a bottom-layer microgrid composed of BESS (Battery energy storage system)s, distributed generators (DGs), and Loads. DG is realized using wind mills. The theory and method of active and reactive power coordinated control before wind speed fluctuations were proposed based on the park transform and Inverse Park transform theory. The real power is increased by the way of optimizing the PWM with an objective function maximization with respect to the real power. The project has been done with a single objective function keeping real power as our target of maximization. The simulation has been done to improve the power quality. Stability issues such as fault clearing time has not been considered in our work.

More over the wind mills are capable of injecting both real and reactive power into the grid, through our work, we extract more real power from the source, keeping the reactive power as it produced early. This is achieved by increasing the total power produced by the wind mill (keeping the reactive power same). The stand-alone control is featured with output voltage and frequency controller that is capable of handling variable load. The potential excess of power is dissipated in the dump-load resistor with the chopper control, and the dc-link voltage is maintained. Dynamic representation of dc bus and small-signal analysis are presented. Simulation results show that the controllers can extract maximum power and regulate the voltage and frequency under varying wind and load conditions. The controller shows very good dynamic and steady-state performance. The simulations had been done with MATLAB ver 7.10 and a related hardware implementation with low power model has been built.

INTRODUCTION

Offshore wind farms (OWFs) are located a distance of less than 25 km away from seashore and an OWF may consist of several high-capacity parallel-operated wind-turbine generators (WTGs). The use of several doubly-fed induction generators (PMSG s) connected directly to a power system is one of the simplest ways of running an OWF due to the advantages of both reactive power control and higher operating efficiency of PMSG s.

This paper presents the results of using a line-commutated HVDC link joined with a modal-control designed damping controller of the rectifier current regulator (RCR) at the rectifier station to perform dynamic-stability enhancement and active-power control of an 80-MW PMSG -based OWF fed to an onshore power grid

The employment of an HVDC link for an OWF has the advantages of fast active-power modulation, effective reactive-power compensation, less voltage drop on an onshore substation, etc. over conventional AC transmission lines. The simulation results of a 200-MW OWF comprising 100 2-MW WTGs connected to a power grid through a multi

IJMTARC – VOLUME – IX – ISSUE – 36, OCT - DEC, 2021

ISSN: 2320-1363

terminal HVDC link with 25 voltage-source converters (VSCs) were presented .

The simulation responses of a 200-MW OWF consisting of 100 individual 2-MW WTGs connected to a power grid through a multi terminal HVDC link with 25 current- source inverters (CSIs) were examined in [2]. The results of a detailed technical-economic analysis of three transmission strategies, i.e., an 150-kV AC system, a 400-kV AC system, and a VSC-HVDC system. On benefits and drawbacks of onshore grid connection of three OWFs of 100 MW, 200 MW, and 500 MW were explored and compared . The control system for a large-scale OWF with an HVDC link using line-commutated converter (LCC) connection to the main onshore network using an aggregate system under both operational and faulted conditions was proposed .

A solution for integrating PMSG based OWFs with a common collection bus controlled by a static synchronous compensator (STATCOM) into a main onshore grid through a line-commutated HVDC link was demonstrated .The control paradigm using the grid frequency control to modulate the rectifier firing angle or the dc-link current to control the power flow of an OWF connected with line commutated HVDC link was proposed.

A frequency controller in the converter to increase the ride-through capability of a VSC-HVDC-based industrial system was presented to exploit the inertia energy of rotating masses in case of voltage disturbances.

Three different frequency controllers and their effects on the voltage-disturbance ride-through capability of a VSC-HVDC-supplied industrial system were proposed .A new concept applicable to large power converters consisting of two series-connected twelve-pulse groups and a new type of converter control applicable to multilevel HVDC schemes with two or more 12-pulse groups per terminal were depicted .

Two types of FACTS devices, a STATCOM and a VSC-HVDC system, were presented to offer a realistic alternative to conventional network reinforcement to solve a range of operational problems in power systems. The operation performance of a wind farm that was made up of several IG-based WTGs and modeled by an equivalent IG incorporated VSC-HVDC was analyzed .

The performance of a VSC-based HVDC link, an HVAC cable interconnection, and a synchronous generator under a faulted condition was compared in [12], and the analyzed results depicted that the VSC-based HVDC link had the ability to provide fault ride-through capability for the studied wind farm comprising IG-based WTGs. An improved model for the transient energy functions of integrated AC/DC power systems involved the omission of DC control dynamics was proposed .

The control requirements of a PMSG -based wind farm connected to a grid through a conventional thyristor based HVDC link were studied. The characteristics of an IG-based OWF connected to a long-distance weak AC grid were explored, and the simulation results demonstrated.

Configuration of the studied 80-MW offshore wind farm connected to an onshore power grid through a line-commutated HVDC link. Proposed HVDC link was able to both supply the variable active power of the OWF to the weak grid and keep the fluctuations of AC voltages at the point of common coupling at an acceptable level .

This project presents damping controller design of RCR, steady-state eigenvalue analysis and transient time-domain simulations of an 80-MW PMSG -based OWF connected to an onshore substation through an HVDC link. System eigenvalues and the design of damping controller of the RCR of the HVDC link are performed under steady-state analysis. Dynamic responses of the studied OWF with and without the designed damping controller of the RCR subject to a torque disturbance are also carried out using time-domain simulations.

EXISITING SYSTEM

IJMTARC – VOLUME – IX – ISSUE – 36, OCT - DEC, 2021

ISSN: 2320-1363

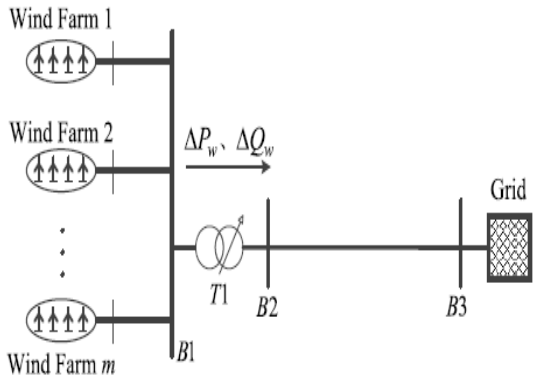

Fig. 1 System under test

1. DFIG based wind farms are available.
2. The control strategy used in earlier systems are like PI, PID, etc.
3. Reactive power compensation is done through TR algorithm.
4. The system is well tested with wind farm connectivity.
5. Power factor maintained in existing work is about 0.95
6. case studies on a sample eight-bus system and a equivalent system, which is a part of an Indian southern grid. The trust region algorithm for determining the optimal settings and the continuation power flow for obtaining the PV curve has been implemented in "FORTRAN" programming language

Significant improvement in voltage stability margins can be attained by appropriate reactive power distribution in the system. Traditionally, reactive power controllers in the system include (but are not limited to) the following:

Generator excitation settings (Vg), switchable VAR Compensator's SVC Q_{SVC}; transformer taps Tt. With an increase in penetration levels and availability of rotor current injection schemes for controlling the reactive power, for a given active power output Q_{wg}, it is possible to control the reactive power output to the desired level (within the capability limits) via appropriate rotor current injection as shown by

$$Q_{wg} = \frac{3}{2}|v|\frac{x_m}{x_{l1}+x_m}\left(\frac{|v|}{x_m} - I_{2d}\right)$$

A family of wind energy systems with integrated functions of active power transfer, reactive power compensation, and voltage conversion under High power penetrations have been addressed.

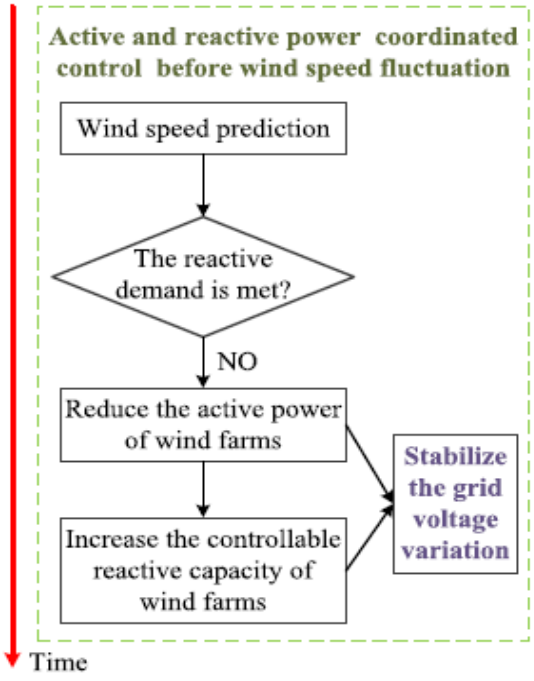

Fig. 2. Flow chart of coordination

PROPOSED SYSTEM

In this project, the new idea of voltage control is proposed based on coordinating active and reactive power before the wind speed fluctuations.

According to the wind speed prediction and the sensitivity matrix, the grid voltage was limited into an allowable range by adjusting the active power of

IJMTARC – VOLUME – IX – ISSUE – 36, OCT - DEC, 2021

ISSN: 2320-1363

Variable speed wind turbines (VSWTs) in advance and fully excavating the controllable reactive capability of VSWTs. The active and reactive power of VSWTs and the grid were optimized by predicting the angle using park transformation

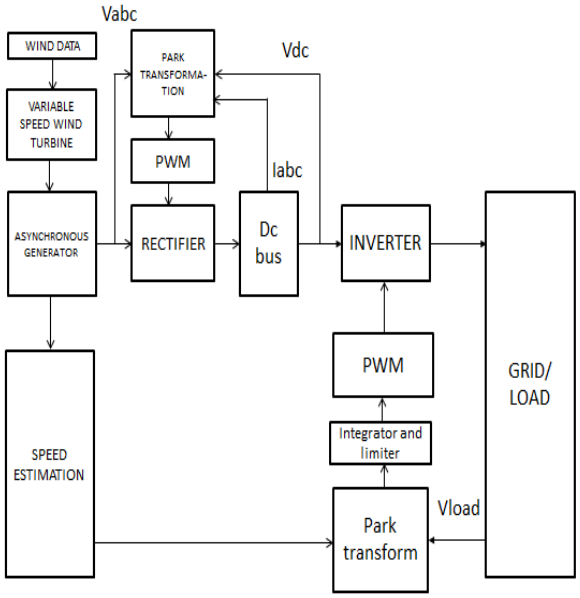

Fig. 3 Block diagram of the system

Park transformation

The Park Transform converts the time-domain components of a three-phase system in an *abc* reference frame to direct, quadrature, and zero components in a rotating reference frame. The transform can preserve the active and reactive powers with the powers of the system in the *abc* reference frame by implementing an invariant version of the Park transform. For a balanced system, the zero component is equal to zero.

$$\begin{bmatrix} d \\ q \\ 0 \end{bmatrix} = \frac{2}{3} \begin{bmatrix} \sin(\theta) & \sin(\theta - \frac{2\pi}{3}) & \sin(\theta + \frac{2\pi}{3}) \\ \cos(\theta) & \cos(\theta - \frac{2\pi}{3}) & \cos(\theta + \frac{2\pi}{3}) \\ \frac{1}{2} & \frac{1}{2} & \frac{1}{2} \end{bmatrix} \begin{bmatrix} a \\ b \\ c \end{bmatrix},$$

where:

a, *b*, and *c* are the components of the three-phase system in the *abc* reference frame.

d and *q* are the components of the two-axis system in the rotating reference frame.

0 is the zero component of the two-axis system in the stationary reference frame.

MODELING OF THE STUDIED SYSTEM

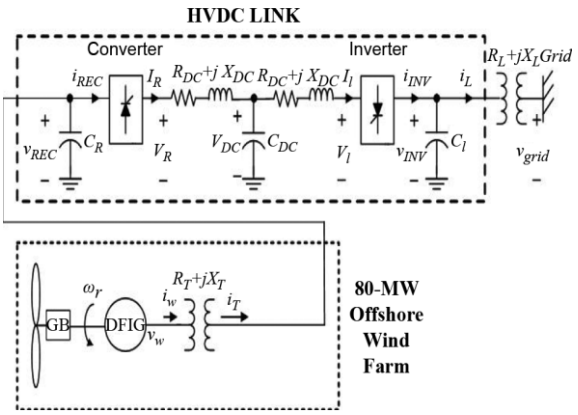

Fig. 4. Configuration of the studied 80-MW offshore wind farm connected to an onshore power grid through a line-commutated HVDC link.

Fig. 4 plots the configuration of the studied 80-MW OWF connected to an onshore power grid through an HVDC link. The 80-MW OWF which is obtained by aggregating 40 2-MW PMSG s is modeled by an equivalent 80-MW PMSG driven by an equivalent variable-speed wind turbine through an equivalent gearbox (GB). The output of the equivalent 80-MW PMSG is connected to the AC input terminals of the HVDC link through a step-up

IJMTARC – VOLUME – IX – ISSUE – 36, OCT - DEC, 2021

ISSN: 2320-1363

transformer and a connection cable. The equivalent impedance of R_T+jX_T shown in Fig. 1 represents the combined impedance of the step-up transformer and the connection cable.

The HVDC link consisting of an AC-to-DC converter, a T-equivalent DC line, and a DC-to-AC inverter delivers the generated power of the PMSG to the onshore power grid through a step-down transformer and an AC transmission line. The impedance of shown in Fig. 1 represents the combined equivalent impedance of the step-down transformer and the AC transmission line. The employed system parameters are listed in the Appendix for conciseness. The mathematical models for the subsystems shown in Fig. 1 are described as below. Except the time variable being in s, the equations depicted below are expressed in per unit (pu) or MKS quantities.

This section presents a unified approach based on modal control theory to design a PID damping controller for the RCR of the proposed HVDC link.

A. Linearized System

The nonlinear system equations developed in the last section are first linearized around a nominal operating point to obtain a set of linearized dynamic system equations of the matrix form:

$$p\mathbf{X} = \mathbf{A}\mathbf{X} + \mathbf{B}\mathbf{U} + \mathbf{V}\mathbf{W}$$
$$\mathbf{Y} = \mathbf{C}\mathbf{X} + \mathbf{D}\mathbf{U} \quad (14)$$

where is the state vector, is the output vector, is the external or compensated input vector, is the disturbance input vector, while , , , and are all constant matrices of proper dimensions. To design the PID damping controller for the RCR of the HVDC link, the variation term and the external input in (14) are appropriately omitted. The state vector can be partitioned into four substate vectors as , where , , , and are referred to the state vectors of the wind PMSG , the transmission line and transformer, the mechanical system of the wind turbine, and the HVDC link, respectively.

Since the wind speed of the studied OWF seldom reaches the rated wind speed of 15 m/s of the WTG, of 12 m/s is properly selected as the operating point for the design of the PID damping controller in the next subsection. The eigen values of the studied OWF with the proposed HVDC link under of 12 m/s are listed in the second column of Table I. An examination of these eigenvalues listed in Table I reveals that the damping of both and can be improved through the addition of the PID damping controller of the RCR to the HVDC link. The PID damping controller of the RCR will be designed by using modal control theory in the next subsection.

B. Design of a PID RCR

The control block diagram of the RCR of the AC-to-DC converter shown in Fig. 7 includes the designed PID damping controller. It is seen that the PID damping controller employs as a feedback signal to generate a damping control signal in order that the damping characteristics of the poorly damped modes listed in Table I can be effectively improved. The block diagram for determining was given in Fig. 7, where the reference value of the output active power can be determined by the rotor speed of the wind PMSG . Hence, the output signal in (14) is

$$\mathbf{Y} = \Delta P \quad (15) \text{ and}$$
$$\mathbf{U} = I_C \quad (16)$$

is the input vector. The transfer function of the proposed PID damping controller in domain is given by

$$H(s) = \frac{\mathbf{U}(s)}{\mathbf{Y}(s)} = \frac{I_C(s)}{\Delta P(s)} = \frac{sT_{WO}}{1+sT_{WO}}\left(K_P + \frac{K_I}{s} + sK_D\right) \quad (17)$$

where , , and are the proportional gain, the integral gain, and the derivative gain of the damping controller, respectively, while is the time constant of the washout term. The four unknown parameters of the PID damping controller can be determined by using modal control theory. The first step is to obtain the state equations in domain by taking Laplace transformation from (14)–(16). The second step is to derive the algebraic equation of the closed-loop system using pole-assignment approach, and the unknown parameters can be directly solved. The input signal in domain can be expressed by

$$\mathbf{U}(s) = H(s)\Delta P(s) = H(s)\mathbf{Y}(s) = H(s)\mathbf{C}\mathbf{X}(s) \quad (18)$$

IJMTARC – VOLUME – IX – ISSUE – 36, OCT - DEC, 2021

ISSN: 2320-1363

Combining (15)–(18), we have

$$s\mathbf{X}(s) = \mathbf{A} + \mathbf{B}[H(s)\mathbf{C}]\mathbf{X}(s) \quad (19)$$

The characteristic equation of the closed-loop system with the designed PID damping controller is given by

$$\det\{s\mathbf{I} - [\mathbf{A} + \mathbf{B}H(s)\mathbf{C}]\} = 0 \quad (20)$$

Since the studied system with the designed PID damping controller of the RCR constitutes a single-input single-output system, (20) is a scalar equation. The parameters of the PID damping controller can then be easily determined by substituting two pairs of pre specified complex-conjugated eigen values corresponding to the assigned poles into (20). Four simultaneous algebraic equations with the four unknowns, , , and , can then be solved to obtain a unique solution. The design results are presented as below. The system eigen values of the studied PMSG -based OWF with the HVDC link and the designed PID damping controller of the RCR are listed in the third column of Table I. It can be obviously discovered from the results listed in Table I that the eigen values of both modes and have been exactly assigned on the desired locations of the complex plane using modal control theory.

STEADY-STATE ANALYSIS

This section examines the effectiveness of the proposed HVDC link joined with the designed PID damping controller of the RCR on dynamic-stability enhancement of the studied PMSG -based OWF. The variations of the four parameters of the designed PID damping controller of the RCR on the closed-loop eigenvalues are also carried out using relative sensitivity coefficients (RSCs).

1) When , the damping of gets better but the damping of becomes worse when wind speed decreases from . The mode changes from two real roots to a pair of complex-conjugated eigenvalues when wind speed drops below 12 m/s and the mode changes from two real roots to a pair of complex-conjugated eigenvalues when wind speed drops to 4 m/s but these two modes still maintain stable. All system modes are located on the left half of the complex plane.

2) When , the damping of becomes better but the damping of still gets worse when wind speed is greater than 12 m/s. Both and maintain two real modes regardless the wind-speed variations. Again, all system eigenvalues are completely positioned on the left half of the complex plane and the system is stable.

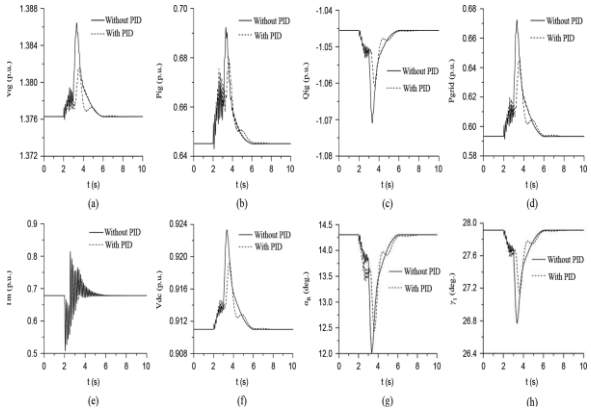

Fig. 5. Dynamic responses of the studied system with and without the designed PID RCR under a pulsed torque disturbance. (a) Terminal voltage of PMSG . (b) Output active power of PMSG . (c) Output reactive power of PMSG . (d) Active power of grid. (e) Mechanical input torque of PMSG . (f) DC-link voltage of DC line. (g) Firing angle of converter. (h) Extinction angle of inverter.

The major constraints for selecting the assigned eigen values for the studied PMSG -based OWF in this paper are analyzed as below.

1) The obtained parameters of the PID damping controller of the RCR should be reasonable. For example, the time constant of the washout term must be positive and the gains of the PID controller should be as small as possible.

2) The eigen values of the closed-loop system including the designed PID damping controller must be completely located on the left half of the complex plane under different operating conditions.

3) The eigen values of the closed-loop system should be insensitive to the variation of all parameters of the designed PID damping controller.

According to 1) the closed-loop eigen values with the designed PID damping controller of the RCR at the selected operating point listed in the third column of Table I, 2) all eigen value results of the closed-loop system under various wind speeds listed in Table II,

IJMTARC – VOLUME – IX – ISSUE – 36, OCT - DEC, 2021

ISSN: 2320-1363

and 3) the designed parameters of the PID damping controller of the RCR, it can be obviously concluded that all system eigenvalues have adequate damping under various wind speeds and the parameters of the designed PID damping controller of the RCR are also appropriate.

TURBINE DETAILS

Wind turbine	
Density of air	1.225 Kg/m^3
Area swept by blades, A	1.06 m^2
Optimum coefficient, K_{opt}	1.67×10^{-3} Nm/(rad/s)^2
Base wind speed	12 m/s
PMSG	
No. of poles	10
Rated speed	153 rad/sec
Rated current	12 A
Armature resistance, R_s	0.425 Ω
Magnet flux linkage	0.433 Wb
Stator inductance, L_s	8.4 mH
Rated torque	40 Nm
Rated power	6 KW

Main electric circuit of the VSI connected to the utility grid

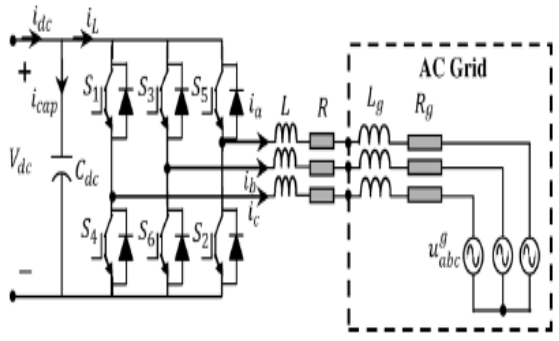

Fig. 6 circuit topology

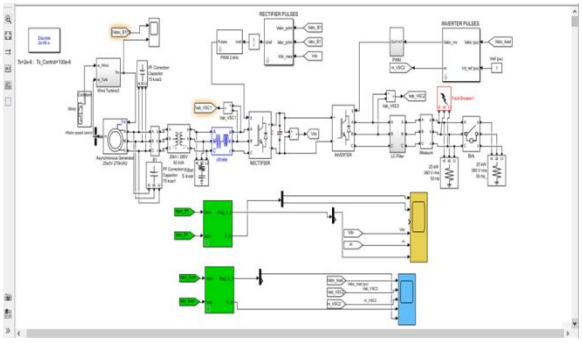

Fig. 7. Simulink model

OUTPUTS (WITHOUT FAULT)

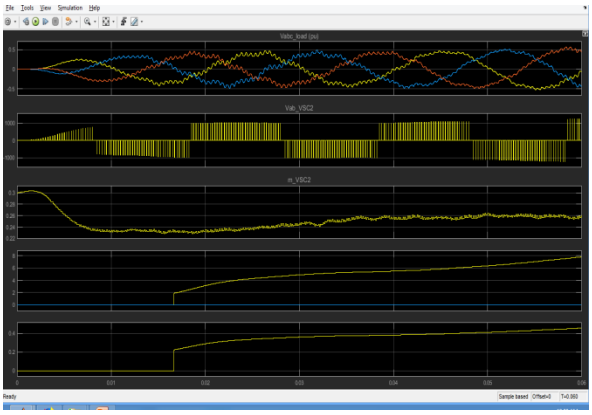

Fig. 8 Simulink outputs - 1

The output waveform shows the real power, reactive power, and DC voltage outputs. Here it may be seen that the real power shown in the PU value. The x axis denotes the time and y axis denotes the concerned parameter.

IJMTARC – VOLUME – IX – ISSUE – 36, OCT - DEC, 2021

ISSN: 2320-1363

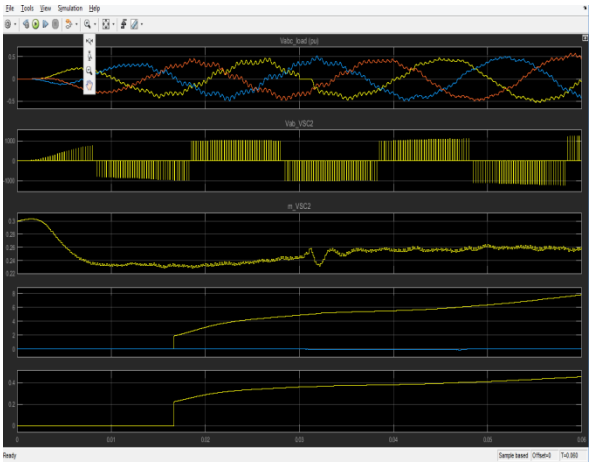

Fig. 9 Simulink outputs - 2

The diagram shown above gives a clear picture of three phase voltage and the inverted voltage without filter. 3rd waveform shows the modulation index. 4th y axis shows the load power (P and Q). whereas the 5th shows the magnitude variation of load voltage.

The simulink model consists of three wind mills constructed using any type of asynchrnous generator, duly constructed with the power level of around 275kVA each and they are energised with a turbine setup. The turbine is rotated using a wind data, which is already stored in the form of mat file. For a nominal power factor correction, the capacitor filter bank is added into the the simulation model. All the power generated are mixed to gether in a common line, where it is next converted into a DC voltage. This DC voltage is further used to convert that into a variable AC, because the input AC power obtained from the wind mills are fluctuating because of variation in the wind speed. The AC to DC conversion is done with a universal bridge, obtained the gate pulses from VSC1. The same is used for injecting the power to the line, where ever a unstable conditions prevails. The DC to AC conversion is done using VSC2, where the control system is applied. Here out target is to maintain the real maximum to the best optimum. This function is like a statcom operation, where the DC energy is again injected in to the line in the form of real or reactive power. The gate pulses generated from park transformation based VSC2 maintains the maximum possible real power. The load at the end of the three phase transmission line is kept at exactly at the set value. The waveforms are observed on the load side and the generator side where ever need to be seen. For convenience, certain blocks are combined together and made as a subsystem. The simulation is run for a time of 0.06. In addition to this, a fault breaker is introduced parallel to the load and analysed for the time taken to return to the healthy state. while a fault occurs. The sampling time as set as 2e-6. Circuit breakers are employed to ensure a constant output even at the absence of the wind power for a short duration. Control system optimizes the gains and hence the final V_{abc} generated is kept as a new reference in order to maximize the real power.

CONCLUSION

This project presented a novel Park transformation based control strategy for the operation of a direct-drive permanent-magnet synchronous generator (or any asynchronous) based stand-alone variable-speed wind turbine. The control strategy for the generator-side converter with maximum power extraction is presented through a voltage source converter at the load side. The real power is increased by the way of optimizing the PWM with an objective function maximization with respect to the real power. The project has been done with a single objective function keeping real power as our target of maximization. A micro controller (89s52) based tiny hardware had been fabricated in order to show the improvement in the output voltage and hence the total power at the load side. This has been done with an inclusion of an inverter circuit for about 100VA at 230V load conditions.

REFERENCES

[1] J. Chow, J. Sanchez-Gasca, H. Ren, and S. Wang, “Power system damping controller design-using multiple input signals,” *IEEE Control Syst. Mag.*, vol. 20, pp. 82–90, Aug. 2000.

[2] M. Aboul-Ela, A. Sallam, J. McCalley, and A. Fouad, “Damping controller design for power system

IJMTARC – VOLUME – IX – ISSUE – 36, OCT - DEC, 2021 ISSN: 2320-1363

oscillations using global signals," *IEEE Trans. Power Syst.*, vol. 11, no. 2, pp. 767–773, May 1996.
[3] I. Kamwa, R. Grondin, and Y. Hebert, "Wide-area measurement based stabilizing control of large power systems—A decentralized/hierarchical approach," *IEEE Trans. Power Syst.*, vol. 16, no. 1, pp. 136–153, Feb. 2001.
[4] Y. Zhang and A. Bose, "Design of wide-area damping controllers for interarea oscillations," *IEEE Trans. Power Syst.*, vol. 23, no. 3, pp. 1136–1143, Aug. 2008.
[5] F. M. Hughes, O. Anaya-Lara, N. Jenkins, and G. Strbac, "Control of DFIG-based wind generation for power network support," *IEEE Trans. Power Syst.*, vol. 20, no. 4, pp. 1958–1966, Nov. 2005.
[6] J. Mauricio, A. Marano, A. Gomez-Exposito, and J. Martinez Ramos, "Frequency regulation contribution through variable-speed wind energy conversion systems," *IEEE Trans. Power Syst.*, vol. 24, no. 1, pp. 173–180, Feb. 2009.
[7] A. E. Leon, J. M. Mauricio, A. Gomez-Exposito, and J. A. Solsona, "An improved control strategy for hybrid wind farms," *IEEE Trans. Sustain. Energy*, vol. 1, no. 4, pp. 131–141, Oct. 2010.
[8] C. Taylor, D. Erickson, K. Martin, R. Wilson, and V. Venkatasubramanian, "WACS-Wide-area stability and voltage control system: R&D and online demonstration," *Proc. IEEE*, vol. 93, no. 5, pp. 892–906, May 2005.
[9] W. Yao, L. Jiang, Q.Wu, J.Wen, and S. Cheng, "Delay-dependent stability analysis of the power systemwith a wide-area damping controller embedded," *IEEE Trans. Power Syst.*, vol. 26, no. 1, pp. 233–240, Feb. 2011.
[10] T. Zabaiou, L.-A. Dessaint, F.-A. Okou, and R. Grondin, "Wide-area coordinating control of SVCs and synchronous generators with signal transmission delay compensation," in *Proc. IEEE Power Energy Soc. Gen. Meeting*, Jul. 2010, pp. 1–9